Research Article

Kurt, B., Investigation of The Potential Inhibitor Effects of Lycorine on Sars-Cov-2 Main Protease (Mpro) Using Molecular Dynamics Simulations and MMPBSA. International Journal of Life Sciences and Biotechnology, 2022. 5(3): p. 424-435. DOI: 10.38001/ijlsb.1110761

Investigation of The Potential Inhibitor Effects of Lycorine on Sars-Cov-2 Main Protease (Mpro) Using Molecular Dynamics Simulations and MMPBSA

Barış Kurt[1*]

ABSTRACT

The main protease (Mpro or 3CLpro) plays important roles in viral replication and is one of attractive targets for drug development for SARS-CoV-2. In this study, we investigated the potential inhibitory effect of lycorine molecule as a ligand on SARS-CoV-2 using computational approaches. For this purpose, we conducted molecular docking and molecular dynamics simulations MM-PB(GB)SA analyses. The findings showed that the lycorine ligand was successfully docked with catalytic dyad (Cys145 and His41) of SARS-CoV-2 Mpro with binding affinity changing between -6.71 and -7.03 kcal mol-1. MMPB(GB)SA calculations resulted according to GB (Generalized Born) approach in a Gibbs free energy changing between -24.925-+01152 kcal/mol between lycorine and SARS-CoV-2 which is promising. PB (Poisson Boltzmann) approach gave less favorable energy (-2.610±0.2611 kcal mol-1). Thus, Entropy calculations from the normal mode analysis (ΔS) were performed and it supported GB approach and conducted -23.100±6.4635 kcal mol-1. These results showed lycorine has a druggable potential but the drug effect of lycorine on COVID-19 is limited and experimental studies should be done with pharmacokinetic modifications that increase the drug effect of lycorine.

ARTICLE HISTORY
Received
28 April 2022
Accepted
13 June 2022

KEYWORDS
Molecular Dynamics Simulation,
MMPBSA,
Gibbs Energy,
SARS-CoV-2

Graphical Abstract

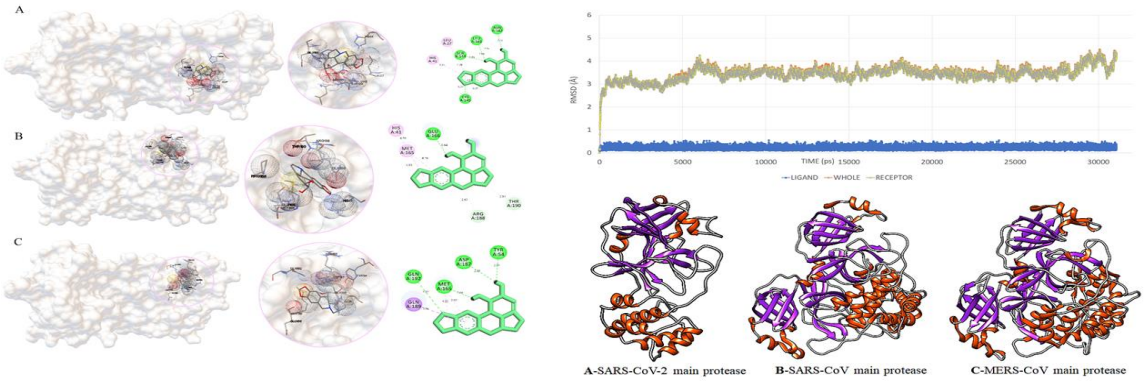

[1] Muş Alparslan University, Faculty of Education, Department of Math, Muş / Turkey
*Corresponding Author: Barış Kurt, e-mail: b.kurt@alparslan.edu.tr

Introduction

Coronaviruses (CoVs) are common pathogens in vertebrates causing various diseases which have been identified as respiratory infections, hepatitis, encephalitis, gastroenteritis [1] and lately COVID-19. The first case of COVID-19 was reported in Wuhan city of Hubei province in China in December 2019 [2] and the outbreak, caused by a novel coronavirus, was declared as global pandemic in 2020 by World Health Organization [3].

The SARS-CoV-2 belonging to β-coronavirus family has an envelope and a non-segmented positive-sense RNA. The genome size of Wuhan-Hu-1 coronavirus (WHCV) is 29.9 kb [4]. The genome encodes 16 non-structural proteins (NSP) along with four structural proteins which are comprised of envelope (E), spike (S) glycoprotein, nucleocapsid (N), and matrix (M) proteins [5]. It is known that ACE-2 (Angiotensin Converting Enzyme-2) receptor is a binding region for SARS-CoV and SARS-CoV-2 viruses [6]. Usually, β-coronaviruses synthesize about 800 kDa long polypeptide [7]. It is determined SARS-CoV-2 is comprised of 16-17 non-structural proteins named as 3-chymotrypsin-like protease ($3CL^{pro}$), papain-like protease (PL^{pro}), helicase, and RNA-dependent RNA polymerase (RdRp). Two proteases ($3CL^{pro}$ and PL^{pro}) serves as probable drug targets since they are of importance in processing two viral proteins in an organized way [8]. Particularly, the $3CL^{pro}$ (main protease or M^{pro}), involved in specific roles in virus replication by cleaving and processing the viral proteins, indicate high-level variations at the 3′ side. In MERS-CoV $3CL^{pro}$, His41 and Ala148 residues have been identified as catalytic dyad [9,10]. On the other hand, Cys145 and His41 are catalytic dyad in SARS-CoV-2 $3CL^{pro}$ [11]. The human CoV (HCoV) 229E M^{pro} contains Cys144 and His41 residues as a catalytic dyad [10].

The sequenced virus RNAs obtained from COVID-19 patients around the world indicated that SARS-CoV-2 have undergone slower mutations compared to other RNA viruses and the rates of SARS-CoV-2 mutations are slower compared to transmission rates of the virus. The slower mutations of the virus emanates from the proofreading mechanism of SARS-CoV-2 and earlier genomic sequencing data of the virus showed that the virus averagely undergoes two-single letter mutations each month [12]. The most significant mutation sites

in virus genome are spike proteins since they help virus to enter into host cells by binding to ACE2 receptors and therefore, is the main target of neutralizing antibodies. Alpha, Beta, Gama and Omicron variants have the mutated sites in their spike proteins rendering them more infectious [12].

Lycorine is a pyrrolo[de]phenanthridine ring-type alkaloid and it is found abundant in plants, belonging to Amaryllidaceae family [13]. Lycorine is known to be cytotoxic compound having anti-tumor effects on different cell lines [14]. Lycorine together with other phytochemicals such as trisphaeridine, homolycorine, and haemanthamine from spring snowflake (*Leucojum vernum*) are found to exhibit high antiretroviral activities with low therapeutic indices (TI_{50} = 1.3 – 1.9) [15] . Particularly, lycorine exhibits virus inhibitory properties against the enterovirus, the flaviviruses, HIV-1, the hepatitis C virus, and the SARS-CoV [15,16] Lycorine, like hemanthamine, inhibits viral activities of the H5N1 influenza strain (highly pathogenic avian influenza virus or HPAIV) by impeding export of virus ribonucleoprotein from nucleus to cytoplasm [17]. Also, lycorine decreases the cytopathic effects of viruses, inhibiting the replication of viruses [18,19]. Lycorine and four herbal extracts are suggested as potential candidates for the treatment of SARS as novel anti-SARS-CoV drugs [20]. Jin et al. [21] stated that lycorine exhibits inhibitory properties against SARS-CoV, MERS-CoV, and SARS- CoV-2 by inhibiting the RNA dependent RNA polymerase (RdRp). However, the effects of lycorine on SARS-CoV or SARS-CoV-2 viruses are more effective than those on MERS-CoV. Likewise, gemcitabine, lycorine, and oxysophoridine in cell culture are reported to show antiviral activities against SARS-CoV-2 [16]. Although these mentioned studies suggest that lycorine is a promising drug candidate, it is still emphasized that further studies are needed to gain more insights into the toxicity and safety profile and antiviral activity of lycorine against SARS-CoV-2. Therefore, in this study, the inhibition potential of lycorine as a promising anti-COVID-19 natural compound was tested on the crystal structure of SARS-CoV-2 main protease ($3CL^{pro}$ or M^{pro}) (PDB ID: 6LU7) using docking and molecular dynamics approaches.

Materials and Methods

Receptor and Ligand Preparation

The ligand lycorine (C16H17NO4) was obtained (Fig. 1) from ZINC (ZINC000003881372) database (https://zinc.docking.org/) (Irwin & Shoichet, 2005). The lycorine includes five rings, 21 heavy atoms, and five hetero atoms. As receptor, the 3D structures of SARS-CoV-2 main protease (referred to as the 3C-like protease) [22] obtained by X-ray diffraction was retrieved from Protein Data Bank (PDB ID: 6LU7) (https://www.rcsb.org/) (Fig. 2). Similarly, SARS-CoV (PDB ID: 1UK3) and MERS CoV (PDB ID: 4WME) main proteases were also retrieved from Protein Data Bank. The 3D models were visualized using UCSF Chimera v1.14 software [23].

Molecular Docking

The AutoDock 4.2 and MGLTools 1.5.6 (24) were used for docking analysis to predict binding scores and modes. To achieve this, the water molecules of the SARS-CoV-2 main protease protein were deleted and polar hydrogens were added to it. The pdbqt file for the protein including Kollman charges was created using MGLTools 1.5.6 [24]. After that, the ligand (the lycorine) was optimized using GAMESS-US software [25] with HF/6-31G+ basis set [26] and the pdbqt file for the ligand including Gastieger charges was generated [24]. The grid box was created with 126x126x126 Å dimensions (grid center x=-26.358 y=15.363 z=60.52) with 0.5694 spacing. Lamarckian genetic algorithm [27] was selected for the docking process. To visualize docking results, Discovery Studio Visualizer [28] and MGLTools 1.5.6 [24] were used.

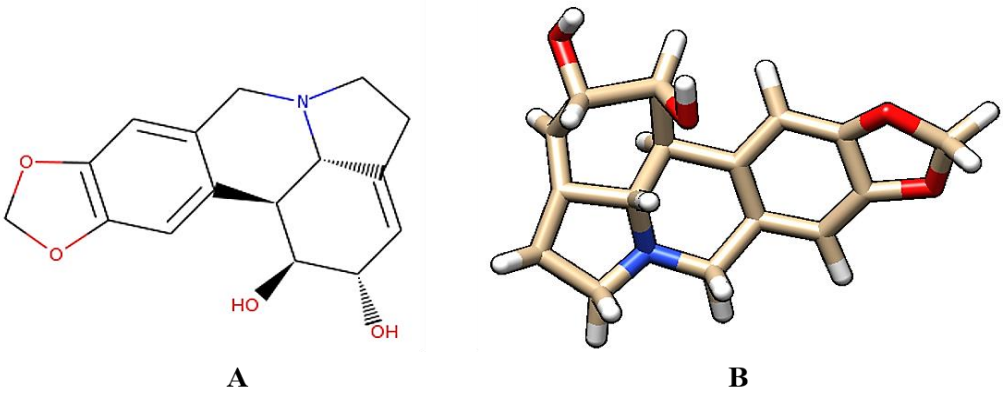

Fig 1. The 2D (A) and 3D structures (B) of lycorine compound

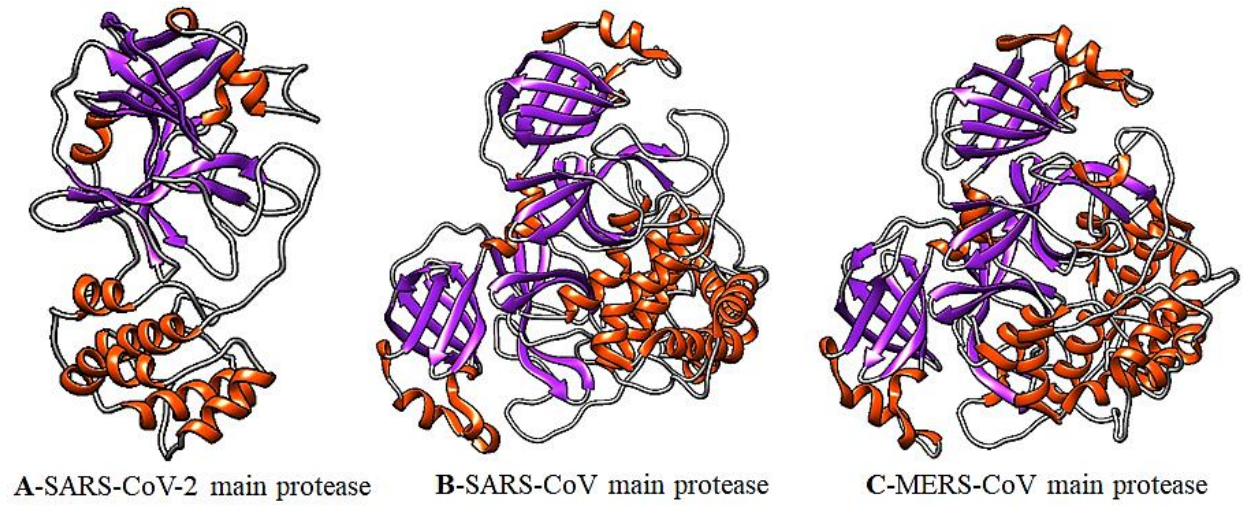

Fig 2. The 3D structure of SARS-CoV-2 (PDB ID: 6LU7), SARS-CoV (PDB ID: 1UK3), and MERS-CoV (PDB ID: 4WME) main proteases. The red, purple, and grey colors show the helices, strands, and coils, respectively. The SARS-CoV-2 showed 95.75% and 95.42% structure overlap with SARS-CoV and MERS-CoV main proteases, respectively (29)

Molecular Dynamics Simulation

After docking process, the lycorine-protein complex with the best docking score was selected for molecular dynamics simulation. The pdb file of this complex was corrected using pdb4amber script in AmberTools 17 package and saved as a new pdb file [30]. Then with tleap program Na^+ ions were added to the complex to provide charge balance and 12 Å TIP3PBOX was used with TIP3P water. AMBER ff14SB and gaff force fields were selected for the protein and the lycorine, respectively [31,32]. To speed up the simulation, after the topology and coordinate files were created, the "hydrogen mass repartitioning" process was applied with the parmed program and the hmassrepartition command [33]. Then two-step minimization was started. In the first step, the complex was restrained, applying 500 kcal mol^{-1}. $Å^2$ force constant. The water molecules were minimized with 1000 steps minimization using the Particle Mesh Ewald (PME) method with 10Å cut-off value. In the second step, force constant was removed from the complex and all system was minimized with the same method as described in the first stage. This time cut-off value was selected as 12Å. Then the heating process was initiated using the Langvein thermostat and selecting SHAKE algorithm while the cut-off value was set to 12Å [30]. Temperature was

increased up to 298K with 1-degree steps. When temperature reached 298K, molecular dynamic simulation was performed for 30 ns with 4 ps relaxation time under 1 atm pressure using the same thermostat and algorithm as mentioned in the heating stage. During the heating and simulation, 10 kcal $mol^{-1}.Å^2$ force constant was applied to the complex. Lastly, deltaG and entropy were calculated using MMPBSA [34] and RMSD value was calculated using cpptraj program [35].

Entropy and Relative Free Energy Calculations Using Molecular Dynamics Simulation

After the simulation, ante-mmpbsa.py program was used to obtain mmpbsa compatible prmtop files for complex consisting of the ligand and the receptor molecules. Mbondi radii was set to 2 as it was recommended in Amber Manual. The free energy of binding is calculated by the following equation [36,37,38,39]:

$$\Delta G_{binding} = \Delta G_{complex} - \Delta G_{receptor} - \Delta G_{ligand} \quad (I)$$

However, since the share of solvent-related energies in the total energy will be greater than the binding energy in solvated states, the solvent effects are included in the calculation and the modified formula is used for the binding free energy [36,37,38,39]:

$$\Delta G^0_{bind,solv} = \Delta G^0_{bind,vacuum} + \Delta G^0_{solv,complex} - (\Delta G^0_{solv,ligand} + \Delta G^0_{solv,receptor}) \quad (II)$$

For hydrophobic contributions, an empirical term is added to the equation after Generalized Born Equation is solved during calculations of solvation free energies [36,37,38]:

$$\Delta G^0_{solv} = G^0_{electrostatic,\varepsilon=80} - G^0_{electrostatic,\ \varepsilon=1} + \Delta G^0_{hydrophobic} \quad (III)$$

The change of Gibbs energy in the vacuum is calculated by the following formula, which also takes into account the average interaction energy and entropy change between the receptor and the ligand [36,37,38]:

$$\Delta G^0_{vacuum} = \Delta E^0_{MM} - T\Delta S^0_{normal\ mode\ analysis} \quad (IV)$$

All energy and entropy calculations were carried out using mmpbsa module in the Amber Tools and the snapshots were taken every 5 ps from the beginning to the end of the simulation.

Results and discussion

Docking analyses

In this study, as a result of molecular docking analyses, it was found that the lycorine molecule was bound to SARS-CoV-2 M^{pro} with binding affinity changing between -6.10 and -7.03 kcal $mol^{-1}$and three different lycorine conformations were detected (Fig. 3). For first conformation, the lycorine was bound to Leu141, Asn142, Ser144, and Cys145 residues of the M^{pro} with -6.71 kcal mol^{-1} docking score. His41, Met165, Glu166, Arg188, and Thr190 were identified as interacting residues in the second conformation with -6.10 docking score whilst Thr54, Met165, Asp187, Gln189, and Gln194 residues were identified as binding sites in the third conformation with -7.03 docking score. Jin et al. [22] reported that substrate-binding pocket of COVID-19 are well-conserved in all M^{pro}s and it shows high potential for drug designing against all CoV-associated diseases. For andrographolide phytochemical from *Andrographis paniculate* (king of bitters), Gly143, Cys145, and Glu166 are the interacting residues for SARS-CoV-2 protease [40]. Cys145 and Glu166 residues were identified in our findings as well. When different phytochemicals in medicinal plants such as isoflavone, myricitrin, methyl rosmarinate, glucopyranoside, calceolarioside, licoleafol, and amaranthin are tested on SARS-CoV-2 CL^{pro} as anti-COVID-19 compounds, two binding sites (His41 and Cys145) are reported as the interacting residues [11]. Consequently, the catalytic dyad (Cys145 and His41) identified in our results also indicate a drug potential of the lycorine against SARS-CoV-2.

Molecular Dynamics Simulation and Energy Calculations

The fact that lycorine has a quite good dock score provides evidence that it may be a good drug candidate. In this regard, molecular dynamics simulation was carried out. The RMSD value was calculated from the simulation with reference to the initial structure (the lowest energy docking complex). Calculated RMSD are shown in Fig. 4. The mean RMSD value during the whole simulation was 3.42 Å for the protein, 3.45 Å for the whole system, and 0.23 Å for the ligand. After 5.8 nanoseconds, it was seen that the RMSD value was fixed and almost unchanged for the protein, while for the ligand this value does not exceed 0.50 Å from the beginning to the end of the simulation. If there were large fluctuations in the

RMSD value, it would indicate that the simulation was stuck at a high energy minimum and therefore, the molecular dynamics simulation should have been continued for a longer period of time. However, the fact that the RMSD value was quite low and remained stable for a long time showed that the simulation progressed quite accurately. Similarly, stabilization in potential energy in Fig. 5 also indicated that the simulation proceeded correctly.

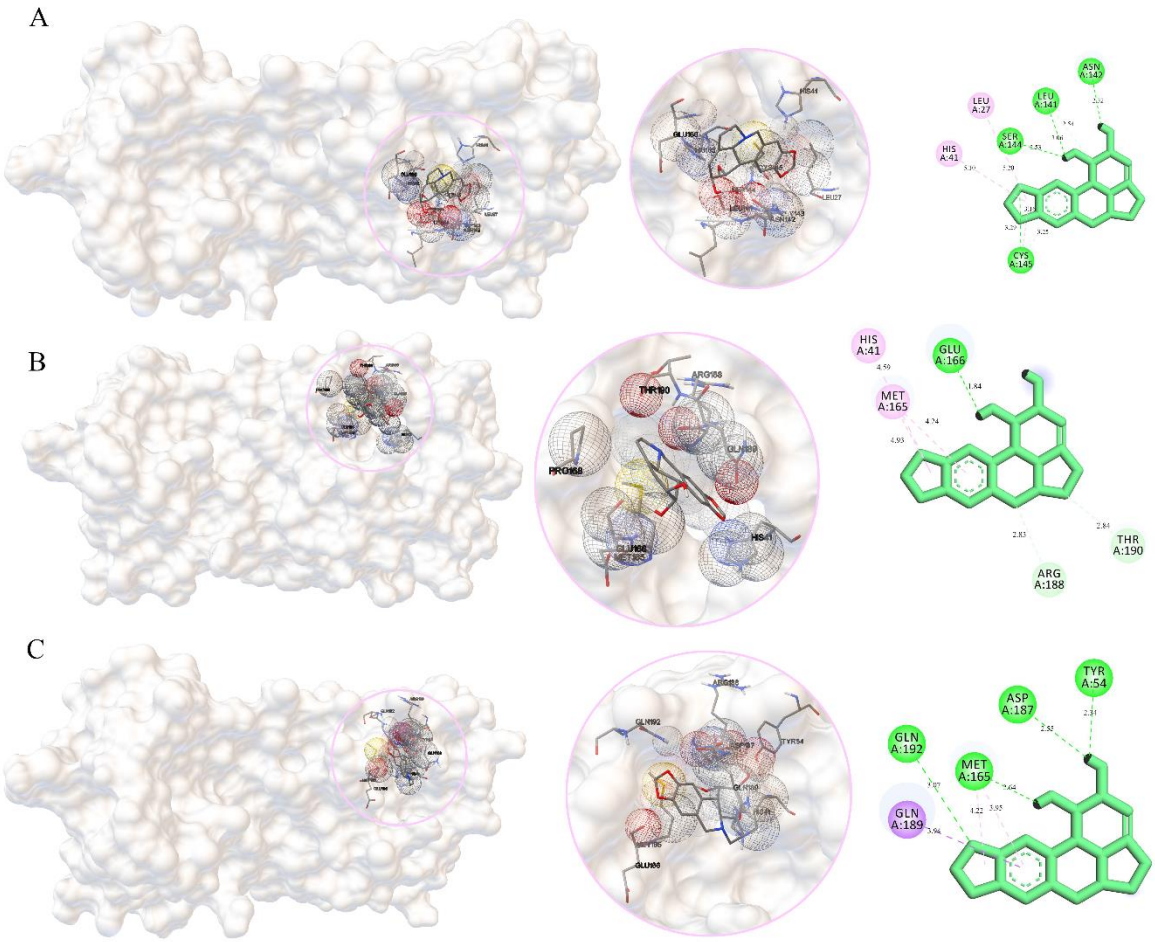

Fig 3. Molecular docking analyses of lycorine ligand with SARSCoV-2 protease with binding affinities of -6.71, -6.10, -7.03 kcal $mol^{-1}$for A, B, and C, respectively.

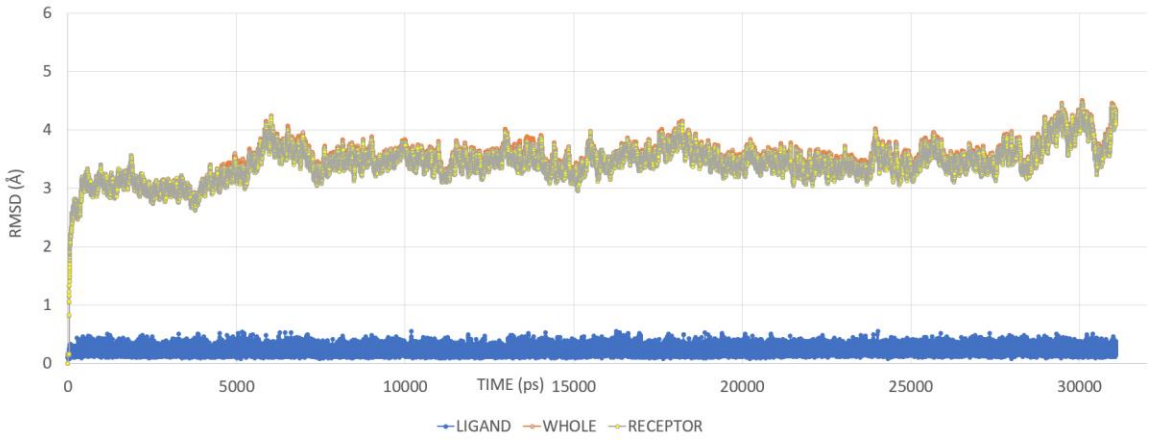

Fig 4. Obtained RMSD value of ligand, receptor, and complex during the simulation

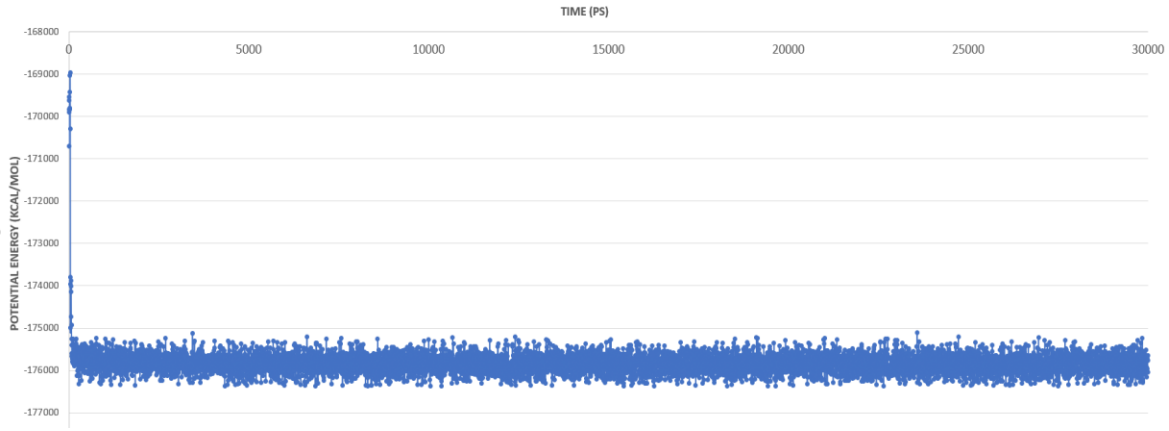

Fig 5. Potential energy profile of lycorine-protein complex

MMPBSA calculations resulted in a Gibbs free energy changing between -24.925±01152 kcal mol^{-1} according to GB (Generalized Born) approach whilst PB (Poisson Boltzmann) approach gives less favorable energy (-2.610±0.2611 kcal mol^{-1}). Entropy calculations from the normal mode analysis (ΔS) were -23.100±6.4635 kcal mol^{-1} (See Supplementary Material for details). When compared with similar studies [41, 42] in the literature, these values are very reasonable for lycorine to be a drug candidate.

Conclusion

The lycorine molecule has a druggable potential for combating SARS-CoV-2. The binding of lycorine molecule to Cys145 and His41 residues, functioning as catalytic dyad in docking analysis, contributes to the druggable potential of this ligand. Energy calculations via molecular dynamics simulations showed that Gibbs Energy was -24.925 ±0.1152 kcal mol^{-1} according to the GB approach and the entropy was -23.100±6.4635 kcal mol^{-1} between SARS-CoV-2 and lycorine. From these results it can be said that even if the drug effect of the lycorine against COVID-19 is limited, its druggable potential is still remarkable. Therefore, it can be suggested that experimental studies should be conducted by employing pharmacokinetic modifications increasing the drug effect of lycorine.

Abbreviations

MMPBSA: Molecular Mechanics Poisson-Boltzmann Surface Area. RMSD: Root Mean Sqaure Deviation. GB: Generalized Born. PB: Poisson Boltzmann

NOTE: Suppl. Inf. Is given below the bibliography

References

1. Weiss, SR., et al., Coronavirus Pathogenesis and the Emerging Pathogen Severe Acute Respiratory Syndrome Coronavirus. Microbiology and Molecular Biology Reviews. 2005. 69(4):635–64.
2. Ji, W., et al., Cross-species transmission of the newly identified coronavirus 2019-nCoV. Journal of Medical Virology. 2020. 92:433–440
3. Cucinotta, D. and M. Vanelli, WHO declares COVID-19 a pandemic. Acta Biomedica. 2020. 91(1):157–60.
4. Wu, F., et al., A new coronavirus associated with human respiratory disease in China. Nature. 2020. 579(7798):265–9.
5. Cui, J., F. Li, and ZL. Shi, Origin and evolution of pathogenic coronaviruses. Nature Reviews Microbiology. 2019. 17(3):181–92.
6. Zhou P, Yang X Lou, Wang XG, Hu B, Zhang L, Zhang W, et al. A pneumonia outbreak associated with a new coronavirus of probable bat origin. Nature. 2020. 579(7798):270–3.
7. Ghosh, AK., et al., Design and synthesis of peptidomimetic severe acute respiratory syndrome chymotrypsin-like protease inhibitors. Journal of Medicinal Chemistry. 2005. 48(22):6767–71.
8. Dömling, A. and L. Gao, Chemistry and Biology of SARS-CoV-2. Chem. 2020. 6(6):1283–95.
9. Needle, D., GT. Lountos, and DS. Waugh, Structures of the Middle East respiratory syndrome coronavirus 3C-like protease reveal insights into substrate specificity. Acta Crystallographica Section D: Structural Biology. 2015. 71:1102–11.
10. Anand, K., et al., (3CL pro) Structure : Basis for Design of Anti-SARS Drugs. Science (80-). 2003. 300(June):1763–7.
11. Tahir-ul Q., et al., Structural basis of SARS-CoV-2 3CLpro and anti-COVID-19 drug discovery from medicinal plants. Journal of Pharmaceutical Analysis. 2020. 4(10) p. 313-319.
12. Callaway E. Beyond Omicron: what's next for COVID's viral evolution. Nature. 2021. 600(7888):204–7.

13. Shen, JW., et al., Lycorine: A potential broad-spectrum agent against crop pathogenic fungi. Journal of Microbiology and Biotechnology. 2014. 24(3):354–8.
14. Shawky, E., In-silico profiling of the biological activities of Amaryllidaceae alkaloids. Journal of Pharmacy and Pharmacology. 2017. 69(11):1592–605.
15. Szlávik, L., and J. Hohman, Alkaloids from Leucojum vernum and antiretroviral activity of amaryllidaceae alkaloids. Planta Medica. 2004. 70(9):871–3.
16. Zhang Y-N., et al., Gemcitabine, lycorine and oxysophoridine inhibit novel coronavirus (SARS-CoV-2) in cell culture. Emerg Microbes & Infections. 2020. 9(1): 1170-1173
17. He. J,, et al., Amaryllidaceae alkaloids inhibit nuclear-to-cytoplasmic export of ribonucleoprotein (RNP) complex of highly pathogenic avian influenza virus H5N1. Influenza Other Respi Viruses. 2013. 7(6):922–31.
18. Yang, L., et al., Tandem mass tag-based quantitative proteomic analysis of lycorine treatment in highly pathogenic avian influenza H5N1 virus infection. PeerJ. 2019(10):1–23.
19. Liu J., et al., Lycorine reduces mortality of human enterovirus 71-infected mice by inhibiting virus replication. Virology Journal. 2011. 8(483):1–9.
20. Li. SY., et al., Identification of natural compounds with antiviral activities against SARS-associated coronavirus. Antiviral Research. 2005. 67(1):18–23.
21. Jin Y., et al., Lycorine, a non-nucleoside RNA dependent RNA polymerase inhibitor, as potential treatment for emerging coronavirus infections. Phytomedicine. 2021. (86):153440.
22. Jin Z., et al., Structure of Mpro from COVID-19 virus and discovery of its inhibitors. Nature. 2020.
23. Pettersen EF., et al., UCSF Chimera -- A visualization system for exploratory research and analysis. Journal of Computational Chemistry. 2004. 25(13):1605–12.
24. Morris, GM., et al., AutoDock4 and AutoDockTools4: Automated Docking with Selective Receptor Flexibility. Journal of Computational Chemistry. 2009. 30:2785–91.
25. Schmidt MW., et al., General atomic and molecular electronic structure system. Journal of Computational Chemistry. 1993. 14(11):1347–63.
26. Pritchard, BP., et al., New Basis Set Exchange: An Open, Up-to-Date Resource for the Molecular Sciences Community. Journal of Chemical Information and Modeling. 2019. 59(11):4814–20.
27. Santos-Martins, D., et al., AutoDock4 and AutoDockTools4: AutoDock4Zn: an improved AutoDock force field for small-molecule docking to zinc metalloproteins. Journal of chemical information and modeling. 2014. 54(8): 2371-2379.
28. Biovia DS., Discovery Studio Visualiser. San Diego: Dassault Systèmes D.S. BIOVIA. 2019.
29. Nguyen MN, Tan KP, Madhusudhan MS. CLICK - Topology-independent comparison of biomolecular 3D structures. Nucleic Acids Res. 2011. 39(SUPPL. 2):24–8.
30. Case DA., et al., Amber 2017 reference manual. Univ California, San Fr. 2017.
31. Wang, J., et al.,Development and testing of a general amber force field. Journal of Computational Chemistry. 2004. 25(9):1157–74.
32. Maier, JA., et al., ff14SB: Improving the Accuracy of Protein Side Chain and Backbone Parameters from ff99SB. Journal of Chemical Theory and Computation. 2015. 11(8):3696–713.
33. Hopkins CW., et al., Long-Time-Step Molecular Dynamics through Hydrogen Mass Repartitioning. Journal of Chemical Theory and Computation. 2015.14. 11(4):1864–74.
34. Miller BR., et al., MMPBSA.py : An Efficient Program for End-State Free Energy Calculations. Journal of Chemical Theory and Computation. 2012. 11. 8(9):3314–21.
35. Roe, DR. and TE. Cheatham, PTRAJ and CPPTRAJ: Software for Processing and Analysis of Molecular Dynamics Trajectory Data. Journal of Chemical Theory and Computation. 2013. 9. 9(7):3084–95.
36. Sharp, KA. and Honig B., Calculating total electrostatic energies with the nonlinear Poisson-

Boltzmann equation. The Journal of Physical Chemistry. 1990 Sep 1. 94(19):7684–92.
37. Tsui, V., and DA. Case, Theory and applications of the Generalized Born solvation model in macromolecular simulations. Biopolymers. 2000. 56(4):275–91.
38. Hou, T., et al., Assessing the Performance of the MM/PBSA and MM/GBSA Methods. 1. The Accuracy of Binding Free Energy Calculations Based on Molecular Dynamics Simulations. Journal of Chemical Information and Modeling. 2011. 24. 51(1):69–82.
39. Murugesan, S., et al., Targeting COVID-19 (SARS-CoV-2) main protease through active phytocompounds of ayurvedic medicinal plants – Emblica officinalis (Amla), Phyllanthus niruri Linn. (Bhumi Amla) and Tinospora cordifolia (Giloy) – A molecular docking and simulation study. Computers in Biology and Medicine. 2021. 136:104683.
40. Enmozhi, SK., et al., Andrographolide As a Potential Inhibitor of SARS-CoV-2 Main Protease: An In Silico Approach. Journal of Biomolecular Structure and Dynamics. 2020.(1):1–10.
41. Gupta, PS., et al., Binding mechanism and structural insights into the identified protein target of COVID-19 and importin-α with in-vitro effective drug ivermectin. Journal of Biomolecular Structure and Dynamics. 2020. 28. 1–10.
42. Bera, K., Binding and inhibitory effect of ravidasvir on 3CL pro of SARS-CoV-2: a molecular docking, molecular dynamics and MM/PBSA approach. Journal of Biomolecular Structure and Dynamics. 2021. 8. 1–8.

SUPPLEMENTARY INFORMATION

ENERGY CALCULATIONS:

GENERALIZED BORN:

Complex:

Energy Component	Average	Std. Dev. Std.	Err. of Mean
VDWAALS	-2595.1594	1.1841	0.1675
EEL	-22016.6765	3.3434	0.4728
EGB	-2671.9663	5.1528	0.7287
ESURF	96.3192	0.0622	0.0088
G gas	-24611.8359	2.5412	0.3594
G solv	-2575.6471	5.192	0.7343
TOTAL	-27187.483	3.5096	0.4963

Receptor:

Energy Component	Average	Std. Dev. Std.	Err. of Mean
VDWAALS	-2558.0203	1.2229	0.173
EEL	-21999.0902	3.3604	0.4752
EGB	-2688.162	5.0578	0.7153
ESURF	97.5587	0.0609	0.0086
G gas	-24557.1105	2.5272	0.3574
G solv	-2590.6033	5.0986	0.7211
TOTAL	-27147.7139	3.4571	0.4889

Ligand:

Energy Component	Average	Std. Dev. Std.	Err. of Mean
VDWAALS	-4.1552	0.014	0.002
EEL	-4.4753	0.0185	0.0026
EGB	-8.6998	0.0122	0.0017
ESURF	2.4862	0.0007	0.0001
G gas	-8.6305	0.0191	0.0027
G solv	-6.2136	0.0122	0.0017
TOTAL	-14.8441	0.021	0.003

Differences (Complex - Receptor - Ligand):

Energy Component	Average	Std. Dev. Std.	Err. of Mean
VDWAALS	-32.984	0.0848	0.012
EEL	-13.1109	0.0826	0.0117
EGB	24.8956	0.12	0.017
ESURF	-3.7257	0.0077	0.001
DELTA G gas	-46.0949	0.103	0.0146
DELTA G solv	21.1699	0.1188	0.0168
DELTA TOTAL	-24.925	0.1152	0.0163

POISSON BOLTZMANN:

Complex:

Energy Component	Average	Std. Dev. Std.	Err. of Mean
VDWAALS	-2595.1594	1.1841	0.1675
EEL	-22016.6765	3.3434	0.4728
EPB	-2316.9485	6.2815	0.8883
ENPOLAR	2305.0838	0.3025	0.0428
EDISPER	-1284.8515	0.4499	0.0636
G gas	-24611.8359	2.5412	0.3594
G solv	-1296.7163	6.3805	0.9023
TOTAL	-25908.5521	4.6694	0.6604

Receptor:

Energy Component	Average	Std. Dev. Std.	Err. of Mean
VDWAALS	-2558.0203	1.2229	0.173
EEL	-21999.0902	3.3604	0.4752
EPB	-2334.0981	6.0497	0.8556
ENPOLAR	2295.5998	0.3327	0.047
EDISPER	-1290.8425	0.453	0.0641
G gas	-24557.1105	2.5272	0.3574
G solv	-1329.3408	6.1589	0.871
TOTAL	-25886.4513	4.4992	0.6363

Ligand:

Energy Component	Average	Std. Dev. Std.	Err. of Mean
VDWAALS	-4.1552	0.014	0.002
EEL	-4.4753	0.0185	0.0026
EPB	-10.7985	0.0121	0.0017
ENPOLAR	30.7347	0.0161	0.0023
EDISPER	-30.7957	0.0669	0.0095
G gas	-8.6305	0.0191	0.0027
G solv	-10.8595	0.073	0.0103
TOTAL	-19.4899	0.0762	0.0108

Differences (Complex - Receptor - Ligand):

Energy Component	Average	Std. Dev. Std.	Err. of Mean
VDWAALS	-32.984	0.0848	0.012
EEL	-13.1109	0.0826	0.0117
EPB	27.9481	0.2788	0.0394
ENPOLAR	-21.2508	0.0421	0.0059
EDISPER	36.7867	0.0795	0.0112
DELTA G gas	-46.0949	0.103	0.0146
DELTA G solv	43.484	0.2707	0.0383
DELTA TOTAL	-2.6109	0.2611	0.0369

ENTROPY CALCULATIONS:

ENTROPY RESULTS (HARMONIC APPROXIMATION) CALCULATED WITH NMODE:

Complex:

Entropy Term	Average	Std. Dev.	Std. Err. of Mean
Translational	17.013	0	0
Rotational	17.7429	0.0033	0.0011
Vibrational	3745.0275	6.2162	1.9657
Total	3779.7833	6.214	1.965

Receptor:

Entropy Term	Average	Std. Dev.	Std. Err. of Mean
Translational	17.0053	0	0
Rotational	17.7351	0.004	0.0013
Vibrational	3725.1792	7.7257	2.4431
Total	3759.9196	7.7257	2.4431

Ligand:

Entropy Term	Average	Std. Dev.	Std. Err. of Mean
Translational	12.7713	0	0
Rotational	10.2045	0.0036	0.0011
Vibrational	19.9878	0.0376	0.0119
Total	42.9637	0.0412	0.013

Differences (Complex - Receptor - Ligand):

Entropy Term	Average	Std. Dev.	Std. Err. of Mean
Translational	-12.7635	0	0
Rotational	-10.1967	0.0049	0.0015
Vibrational	-0.1395	6.4631	2.0438
DELTA S total=	-23.1	6.4635	2.0439